

A dual role of the ribosome-bound chaperones RAC/Ssb in maintaining the fidelity of translation termination

Anne-Sophie Gribling-Burrer¹, Marco Chiabudini¹, Ying Zhang¹, Zonghao Qiu¹,
Mario Scazzari¹, Tina Wölfle¹, Daniel Wohlwend² and Sabine Rospert^{1,3,*}

¹Institute of Biochemistry and Molecular Biology, ZBMZ, Medical Faculty, University of Freiburg, D-79104 Freiburg, Germany, ²Institute of Biochemistry, Chemical and Pharmaceutical Faculty, University of Freiburg, D-79104 Freiburg, Germany and ³BIOSS Centre for Biological Signaling Studies, University of Freiburg, D-79104 Freiburg, Germany

Received January 17, 2019; Revised April 05, 2019; Editorial Decision April 22, 2019; Accepted April 25, 2019

ABSTRACT

The yeast ribosome-associated complex RAC and the Hsp70 homolog Ssb are anchored to the ribosome and together act as chaperones for the folding and co-translational assembly of nascent polypeptides. In addition, the RAC/Ssb system plays a crucial role in maintaining the fidelity of translation termination; however, the latter function is poorly understood. Here we show that the RAC/Ssb system promotes the fidelity of translation termination via two distinct mechanisms. First, via direct contacts with the ribosome and the nascent chain, RAC/Ssb facilitates the translation of stalling-prone poly-AAG/A sequences encoding for polylysine segments. Impairment of this function leads to enhanced ribosome stalling and to premature nascent polypeptide release at AAG/A codons. Second, RAC/Ssb is required for the assembly of fully functional ribosomes. When RAC/Ssb is absent, ribosome biogenesis is hampered such that core ribosomal particles are structurally altered at the decoding and peptidyl transferase centers. As a result, ribosomes assembled in the absence of RAC/Ssb bind to the aminoglycoside paromomycin with high affinity ($K_D = 76.6$ nM) and display impaired discrimination between stop codons and sense codons. The combined data shed light on the multiple mechanisms by which the RAC/Ssb system promotes unimpeded biogenesis of newly synthesized polypeptides.

INTRODUCTION

Faithful interpretation of the genetic code is essential for the synthesis of functional proteins in living cells. Assem-

bly of these extraordinary molecular machines proceeds via a complex multistep pathway that requires more than 200 assembly factors and 76 small nucleolar RNAs (snoRNAs) (1,2). Improper assembly, due to defects in core ribosomal components or in the assembly machinery, impacts on the efficiency and fidelity of translation (1,3). In humans, ribosome assembly defects, if not lethal, are consistently linked to inherited diseases, such as neurodegenerative disorders, cancers or myopathies (4).

One essential aspect of translational fidelity is the proper recognition of stop codons, which is mediated by the release factors eRF1/eRF3 in eukaryotic cells (3,5,6). Occasionally, a stop codon is not recognized properly. Instead, a near-cognate tRNA is accommodated in the ribosomal A-site (3,7). This leads to stop codon readthrough and produces C-terminally extended polypeptides that are released when the ribosome encounters the next *in frame* stop codon (3,7). On the other hand, termination can erroneously occur during translation elongation, even when the A-site contains a sense codon (3,8,9,10,11,12). This type of mechanistically poorly defined fidelity problem, termed ribosome drop-off or premature translation termination, leads to the release of C-terminally truncated polypeptides. C-terminally extended as well as C-terminally truncated polypeptides are oftentimes non-functional or even detrimental to a cell.

Yeast contains a specialized chaperone system composed of the functionally redundant Hsp70 isoforms Ssb1 and Ssb2 (collectively termed Ssb) and the ribosome associated complex (RAC) comprising the Hsp70 Ssz1 and the Hsp40 Zuo1. Together, these proteins form a functional chaperone unit (termed the RAC/Ssb system) (13,14). Both, Ssb and RAC, bind to the ribosome directly and possess domains localized close to the ribosomal tunnel exit, where Ssb contacts emerging nascent chains in a RAC-dependent manner (13,14,15). When bound to translating ribosomes,

*To whom correspondence should be addressed. Sabine Rospert. Tel: +49 761 203 5259; Fax: +49 761 203 5257; Email: sabine.rospert@biochemie.uni-freiburg.de

the RAC/Ssb system is involved in co-translational protein folding (13,14,16,17) and the co-translational assembly of multi-protein complexes (18).

Besides its function in co-translational protein folding the RAC/Ssb system affects ribosome biogenesis at multiple levels. First, RAC/Ssb plays a direct role in the nuclear steps of ribosome assembly. To that end, a fraction of Zuo1 localizes to the nucleolus where it interacts with ribosome assembly intermediates and together with Ssb assists ribosome biogenesis (19). Ssb contains a nuclear export signal (20), which is likely involved in the export of 60S subunits from the nucleus (19). Second, RAC/Ssb is required for proper signaling via the TORC1-Sch9 axis, which warrants sufficient ribosome production of fast growing yeast cells in glucose-rich conditions (21). Due to its multiple functions in ribosome biogenesis, cells lacking RAC/Ssb contain a reduced number of ribosomes (13,14,22,23), display enhanced aggregation of ribosomal particles (19,23,24), and severe defects in pre-rRNA processing (19,23).

Phenotypically, deletion of *ZUO1*, *SSZ1*, or simultaneous deletion of *SSB1* and *SSB2* results in a nearly identical set of pleiotropic phenotypes such as slow growth, sensitivity against cold, high salt and aminoglycosides, as for example paromomycin (13,14). Paromomycin binds with high affinity to helix 44 (h44) at the decoding center of prokaryotic ribosomes causing reduced fidelity of translation elongation and termination (3,25,26). Paromomycin also binds to eukaryotic ribosomes, not specifically to h44, but rather to multiple low affinity binding sites (27). Remarkably, the IC_{50} of paromomycin is enhanced about 100-fold when yeast cells lack a functional RAC/Ssb system (28).

Indeed the RAC/Ssb system is also required to maintain translational fidelity. In the absence of RAC/Ssb stop codon readthrough is enhanced (3,28,29). On the other hand RAC/Ssb prevents ribosome drop-off when ribosomes struggle with the translation of polylysine segments encoded by *AAG* or *AAA* (poly-*AAG/A* sequences). Enhanced ribosome drop-off in the absence of RAC/Ssb is independent of the ribosome-associated protein quality control machinery, however, depends on the small ribosomal subunit protein Asc1 (8,30). Two possible scenarios may account for this unusual observation: In one, release of C-terminally truncated polypeptides may be due to premature translation termination occurring on ribosomes stalled with an *AAA* or *AAG* codon in the A-site (8) (Supplementary Figure S1A); in the other, release of C-terminally truncated polypeptides may be due to ribosome sliding on poly-*AAG/A* sequences, which leads to *reading frame* switches, such that *out-of-frame* stop codons can induce canonical translation termination (31) (Supplementary Figure S1B).

In an attempt to understand how RAC/Ssb impacts on the different aspects of translation termination at a mechanistic level we first revisited the question of polypeptide release during translation of poly-*AAG/A* sequences. Our data reveal that premature polypeptide release in the absence of RAC/Ssb was not connected to ribosome sliding into an alternative *reading frame*. Rather, translation of poly-*AAG/A*, which is slow in the wild-type, was further slowed down in the absence of RAC/Ssb, facilitating non-canonical polypeptide release at lysine codons *in vivo*.

Stalling on poly-*AAG/A* was directly affected by RAC/Ssb, indicating that the interaction of RAC/Ssb with the ribosome facilitated translation of a stalling-prone transcript. In contrast, enhanced stop codon readthrough in the absence of RAC/Ssb was not connected to a direct effect of the chaperone system during translation, but was the result of structural alterations within core ribosomal particles assembled in cells lacking RAC/Ssb. Structural alterations concerned functionally important sites within the decoding center and peptidyl transferase center (PTC) and strongly enhanced the affinity of ribosomal particles for paromomycin.

MATERIALS AND METHODS

Yeast strains, plasmids and media

The wild-type strain was MH272-3f α (*ura3*, *leu2*, *his3*, *trp1*, *ade2*) (32). Δ *zuo1*, Δ RAC/Ssb (Δ *zuo1* Δ *ssz1* Δ *ssb1* Δ *ssb2*) (15,28,33), Δ *hbs1*, Δ *dom34*, Δ *zuo1* Δ *dom34* and Δ *zuo1* Δ *hbs1* (8,34) were previously described. Δ *hel2* and Δ *zuo1* Δ *hel2* were constructed by replacing the *HEL2* *orf* in the wild-type or Δ *zuo1* strains with the *Schizosaccharomyces pombe his5⁺* marker cassette, which complements the *Saccharomyces cerevisiae his3* mutation (35). Yeast strains were grown in YPD complete medium (1% yeast extract, 2% peptone, 2% glucose), or in SD minimal medium (6.7 g/l yeast nitrogen base without amino acids, 2% glucose) supplemented with the appropriate amino acids. Cultures were grown in liquid medium at 30°C with constant shaking at 200 rpm. Luc-K12-3HA was expressed from the 2 μ plasmid pYEplac195-Luc-K12-3HA under control of the *ZUO1* promoter as previously described (8). Luc-K12-3HA contains the (*AAG-AAG-AAA*)₄ sequence and four *out-of-frame* stop codons (*ofs*). For clarity the original Luc-K12-3HA (8) in some experiments is termed Luc-K12(*AAG/A*)₁₂-3HA-4-*ofs* (see Supplementary Figure S1C). The other Luc-K12-3HA constructs are based on Luc-K12(*AAG/A*)₁₂-3HA-4-*ofs*, in which the (*AAG-AAG-AAA*)₄ sequence was replaced with (*AAA*)₁₂ (Luc-K12(*AAA*)₁₂-3HA) or (*AAG*)₁₂ (Luc-K12(*AAG*)₁₂-3HA). Silent mutations with respect to the 3HA sequence were employed to remove either two or four *out-of-frame* stop codons, resulting in Luc-K12(*AAG/A*)₁₂-3HA-2-*ofs*, Luc-K12(*AAA*)₁₂-3HA-2-*ofs* and Luc-K12(*AAG/A*)₁₂-3HA-0-*ofs* (Supplementary Figure S1C). Luc-K12-stop-3HA contains an *in frame* stop codon, resulting in the expression of a polypeptide lacking the 3HA tag, which is shortened by 29 residues (Supplementary Figure S1C). Reporter constructs for *in vitro* transcription are based on pSPUTK (taxonomy ID: 201027). The *in vitro* transcribed reporter mRNAs are termed mHis3-ss, mHis3-ws, mHis3-K20-3HA-ss, mHis3-K20-3HA-ws, mHis3-K20-3HA-4s, mGlk1-K20-2HA-ss and mGlk1-stop-K20-2HA-ss. For details on the reporter sequence see Supplementary Figures S1C, S2A–C and S4A.

Quantification of luciferase translation products

Total protein extracts for immunoblotting analysis were prepared by the method of Kushnirov (36). Relative amounts of full length luciferase (FL) and C-terminally

shortened luciferase species (SF) were detected via immunoblotting, which were analyzed in two different dilutions and two different exposure times of a single immunoblot. Quantifications were performed with at least three independent biological samples. Immunoblot quantification was performed using AIDA Image Analyzer software (Raytest).

Ribosome sedimentation assays

Ribosome sedimentation assays were employed to separate total cell extract into a cytosolic supernatant and a ribosomal pellet as described (8). In brief, after collecting cells in the presence of 100 $\mu\text{g/ml}$ cycloheximide, extracts were prepared by glass bead disruption in 20 mM HEPES-KOH pH 7.4, 120 mM KOAc, 2 mM $\text{Mg}(\text{OAc})_2$, 2 mM dithiothreitol (DTT), 100 $\mu\text{g/ml}$ cycloheximide, 1 mM phenylmethylsulfonyl fluoride (PMSF), 1 \times protease inhibitor mix. Samples corresponding to 0.5 A_{260} units in a total volume of 60 μl were loaded onto a 90 μl low salt (25% sucrose, 20 mM HEPES-KOH, pH 7.4, 120 mM KOAc, 2 mM $\text{Mg}(\text{OAc})_2$, 2 mM DTT, 1 mM PMSF, 1 \times protease inhibitor mix) or high-salt (25% sucrose, 20 mM HEPES-KOH, pH 7.4, 800 mM KOAc, 2 mM $\text{Mg}(\text{OAc})_2$, 2 mM DTT, 1 mM PMSF, 1 \times protease inhibitor mix) sucrose cushion. Ribosomes were collected by ultracentrifugation (30 min, 350 000 $\times g$, 4°C, TLA-100, Beckmann). Aliquots of total, supernatant, and pellet were analyzed via sodium dodecyl sulphate-polyacrylamide gelelectrophoresis (SDS-PAGE) followed by immunoblotting.

In vitro transcription and translation

Yeast translation extract (YTE) was prepared as previously described (37) from wild-type or the Δzuo1 strain. DNA templates for transcription reactions were generated by polymerase chain reaction using Taq DNA polymerase. mRNAs were generated using SP6 polymerase (ThermoFischer Scientific). $m^7\text{G-cap}$ was added co-transcriptionally using the $m^7\text{G}(5')\text{ppp}(5')\text{G RNA Cap Structure Analog}$ (NEB) according to the manufacturer's instructions. Transcripts were purified using the RNeasy Mini kit (Qiagen) followed by phenol-chloroform extraction and ethanol precipitation. Prior to use, the quality of the transcripts was controlled on 3.5% urea-polyacrylamide gels (38). Translation reactions were performed at 20°C as previously described (37,39) in translation buffer (final concentration 1.0 mM adenosine triphosphate, 0.08 mM guanosine triphosphate (GTP), 17.5 mM creatine phosphate, 0.2 mg/ml creatine phosphokinase, 0.2 mM of each of the 19 amino acids (excluding methionine), 2.2 mM putrescine, 0.1 mg/ml yeast tRNA, 0.5 mCi/ml [^{35}S]-methionine (1000 Ci/mmol, PerkinElmer Life Science), 100 U/ml RNaseOUT (Invitrogen), 0.1 μM mRNA and 35% YTE. At the indicated time points, samples were removed from the translation reaction and were precipitated with 5% trichloroacetic acid (TCA). TCA-precipitated pellets were resuspended in SDS-PAGE sample buffer at 95°C and were then separated on 10% Tris-Tricine polyacrylamide gels (40). For the detection of peptidyl-tRNAs, TCA precipitation was performed for 10 min on ice and TCA pellets were subsequently resuspended in SDS-PAGE sample buffer at 40°C and were then

analyzed on 8% Bis-Tris SDS polyacrylamide gels (stacking gel: 0.36 M Bis-Tris pH 6.8, 4% (w/v) acrylamide, 0.27% (w/v) $\text{N,N}'$ -methylenebisacrylamide; separating gel: 0.36 M Bis-Tris pH 6.8, 7.8% (w/v) acrylamide, 0.52% (w/v) $\text{N,N}'$ -methylenebisacrylamide) at 140 mA/h in MOPS running buffer (50 mM MOPS, 50 mM Tris-HCl, 1 mM ethylenediaminetetraacetic acid, 0.1% (w/v) SDS, 5 mM sodium bisulfite). Gels were dried and subsequently analyzed via autoradiography.

Toeprinting analysis

Toeprinting was performed as described (41), with minor modifications. Briefly, *in vitro* translation reactions were performed as described in the previous section except that 40 μM of cold methionine was added instead of [^{35}S]methionine. After 60 or 90 min of translation at 20°C, cycloheximide was added to a final concentration of 300 $\mu\text{g/ml}$ to stabilize translational complexes, which were then collected by ultracentrifugation at 400 000 $\times g$ for 25 min at 4°C. Ribosomal pellets were resuspended directly in annealing buffer (final concentration 60 mM Tris-HCl pH 8.0, 90 mM KCl, 10 mM MgCl_2 , 10 mM DTT, 0.3 mM dNTPs and 1 U/ μl RNaseOUT), and were heated for 2 min at 55°C (41). As a control, ribosomes were blocked at the initiation codon by adding 300 $\mu\text{g/ml}$ cycloheximide (final concentration) to the translation reactions prior to addition of mRNA. Translation complexes were subsequently analyzed by primer extension using 20 000 cpm/ μl of [^{32}P]-labeled primer complementary to the 2HA tag sequence (CGTATGGATAGGAACCTGC) of the mGlk1-K20-2HA-ss reporter, and 5 U/ μl of SuperScript IV reverse transcriptase (Invitrogen) at 37°C for 30 min. After phenol-chloroform extraction and ethanol precipitation, reaction products were separated on 7.5% urea-polyacrylamide gels and were visualized using a BioRad PhosphorImager.

Ribosome purification

Yeast cultures grown in YPD to $\text{OD}_{600} = 1.2$, were harvested by centrifugation and washed with ice-cold water. The resulting cell pellets were resuspended in 3.5 ml/g cells of sorbitol buffer (50 mM potassium-phosphate buffer pH 7.4, 1.4 M sorbitol, 10 mM DTT) and were treated with 2.5 mg/g cells zymolyase for 35 min at 30°C. Subsequently, spheroblasts were collected, washed with cold sorbitol buffer and were lysed using a Dounce homogenizer. Cell lysates were clarified by two rounds of centrifugation at 4°C. A first round at 15 000 rpm (SS-34 rotor) for 18 min and a second round at 38 000 rpm (Ti70.1 rotor) for 35 min. To collect ribosomes, clarified supernatants were loaded onto high-salt sucrose-cushions (50 mM HEPES-KOH pH 7.4, 800 mM KOAc, 2 mM $\text{Mg}(\text{OAc})_2$, 1 mM PMSF, 25% sucrose, 1 \times protease inhibitor cocktail (Sigma)) which were centrifuged for 25 min at 95 000 rpm, 4°C (MLA130 rotor). Ribosomal pellets were resuspended in ribosome buffer (20 mM HEPES-KOH pH 7.4, 120 mM KOAc, 2 mM $\text{Mg}(\text{OAc})_2$, 5% glycerol). For Isothermal Titration Calorimetry (ITC) analysis, ribosomes were dialyzed overnight against ribosome buffer at 4°C.

Ribosomal RNA structure probing by chemical modification

Purified ribosomes (concentration 1 μM) were incubated with 45 mM dimethyl sulfate (DMS) in a volume of 25 μl of DMS reaction buffer (30 mM HEPES-KOH pH 7.5, 3 mM $\text{Mg}(\text{OAc})_2$, 100 mM KCl, 2 mM DTT) for 8 min at 26°C. After adding 475 μl DMS stop buffer (30% β -mercaptoethanol in 0.3 M NaOAc pH 5.2), ribosomes were precipitated with one volume of isopropanol. To remove ribosomal proteins, ribosomal pellets were resuspended in 250 μl proteinase K buffer (50 mM Tris-HCl pH 7.5, 20 mM NaCl, 1% SDS, 8 U/ml Proteinase K) and were incubated at 37°C for 30 min. After phenol-chloroform extraction and ethanol precipitation in the presence of 0.2 M NaCl, rRNA pellets were dried and resuspended to a final concentration of 1 $\mu\text{g}/\mu\text{l}$ in dH_2O . For the analysis of m^7G modifications, further cleavage steps were performed as described (42,43). Briefly, 10 μg of DMS-modified rRNA was incubated with 250 mM NaBH_4 for 30 min in the dark on ice. Samples were then ethanol-precipitated and pellets were directly resuspended in 20 μl of 1 M aniline acetate pH 4.5 ($\text{H}_2\text{O}:\text{AcOH}:\text{aniline} = 7:3:1$) and were incubated in the dark for additional 20 min at 60°C. After ethanol-precipitation, pellets were resuspended to a final concentration of 0.5 $\mu\text{g}/\mu\text{l}$ in dH_2O . Primer extension and RNA sequencing reactions were performed with 2 μg rRNA using AMV reverse transcriptase (Promega) with [^{32}P]-end-labeled primers (200 000 cpm) complementary to either the 18S (primer 18S: GAGTTGCCCTTCTCTAAG) or 25S (primer 25S: GGTATGATAGGAAGAGC) yeast rRNA region of interest at 42°C for 30 min. After ethanol precipitation, reaction products were separated on 7.5% urea-polyacrylamide gels and were visualized using a BioRad PhosphorImager.

Isothermal titration calorimetry (ITC)

ITC experiments were performed with a Microcal VP-ITC microcalorimeter (Malvern Instruments, Germany) at 289 K using ribosome concentrations between 3.5 and 5 μM in the sample cell and paromomycin (Sigma) concentrations between 60 and 100 μM in the injection syringe. Concentrations were determined gravimetrically (paromomycin) and by the native absorption coefficient at 280 nm wavelength (ribosomes). Data were obtained in discrete titration experiments with an injection volume of 13.6 μl per injection. Subsequently, automated baseline correction, integration of heats per injection and normalization against the molar concentrations were done with NITPIC (44,45). Data were globally fitted according to a $\text{A} + \text{B} \rightleftharpoons \text{AB}$ binding model with SEDPHAT (46). The validity of the fitting procedure was assessed by one-dimensional error surface projections at a P-level of 0.95 for both ΔH and K_D . At last, binding isotherms and fits were plotted with GUSI (47).

Miscellaneous

Proteins were separated on 10–12% Tris-Tricine gels for immunoblotting with rabbit polyclonal antibodies (Rospert lab antibody collection, generated by Eurogentec) and were developed by enhanced chemiluminescence as previously

described (8). Polyclonal rabbit anti-luciferase antibody (α -Luc) was purchased from Sigma (L0159). RAC was purified as previously described (15). Protease inhibitor mix (1 \times) contained 1.25 $\mu\text{g}/\text{ml}$ leupeptin, 0.75 $\mu\text{g}/\text{ml}$ antipain, 0.25 $\mu\text{g}/\text{ml}$ chymostatin, 0.25 $\mu\text{g}/\text{ml}$ elastinal, 5 $\mu\text{g}/\text{ml}$ pepstatin A.

RESULTS

Premature translation termination *in vivo* does not involve ribosome sliding on poly-AAG/A sequences

To test for codon-dependent ribosome stalling during translation of polylysine segments in yeast, we employed the Luc-K12-3HA reporter, in which luciferase (Luc) and a 3HA tag (3HA) are fused *in frame* via a stalling sequence encoding for 12 lysine residues (K12) (Figure 1A) (8). We previously demonstrated that in the absence of functional RAC/Ssb, expression of a Luc-K12-3HA reporter in which K12 is encoded by $(\text{AAG-AAG-AAA})_4$ gives rise to a C-terminally shortened fragment (K12-SF), which is released from the ribosome *in vivo* in an eRF3-dependent manner (8 and Supplementary Figure S1A). Here, we analyzed additional Luc-K12-3HA reporters, with K12 encoded by $(\text{AAG-AAG-AAA})_4$, $(\text{AAA})_{12}$, or $(\text{AAG})_{12}$ (collectively termed poly-AAG/A sequences) and, as a control, Luc-N12-3HA containing $(\text{AAC})_{12}$ encoding for 12 asparagines (N12). In the wild-type and Δzuo1 strains, expression of Luc-N12-3HA produced only full length translation product (N12-FL) (Figure 1B). Expression of the different Luc-K12-3HA reporters in the wild-type produced mainly full length protein (K12-FL) (Figure 1B). As expected, expression of the Luc-K12-3HA reporters in the Δzuo1 strain produced a significant amount of K12-SF (8) (Figure 1B). K12-SF expression was codon dependent with an about 2-fold increased level of K12-SF from the $(\text{AAA})_{12}$ reporter, indicating that premature nascent polypeptide release in the absence of RAC/Ssb was affected by the codon usage (Figure 1B and C). The *in vivo* origin of truncated protein species is complex, because stalling of ribosomes on poly-AAG/A sequences induces endonucleolytic cleavage of a fraction of the mRNA molecules generating stop codon-less transcripts (8,48,49). If these stop codon-less transcripts escape degradation they are translated into C-terminally truncated protein species, which are released from ribosomes via the eRF1/eRF3-homologs Dom34/Hbs1 (8,49). To assess if codon usage exerted a significant effect on endonucleolytic cleavage and/or Dom34/Hbs1-dependent release we tested expression of the $(\text{AAA})_{12}$ -encoded Luc-K12-3HA reporter in strains lacking Dom34 or Hbs1 as well as the RAC/Ssb system (Supplementary Figure S1D). Consistent with our previous analysis (8) K12-SF was expressed independently of the Dom34/Hbs1 system (Supplementary Figure S1D).

Besides the well-studied -1 and $+1$ frameshifting events (50), ribosomes dramatically change their initial frame during translation of iterated AAA sequences in a process termed ribosome sliding (31,51,52) (Supplementary Figure S1B). Ribosome sliding can occur on poly-AAG/A sequences, but is most efficient during the translation of polyA (31,51,52). The 3HA tag of the Luc-K12-3HA reporter contains 4 out of frame stop codons (*ofs*) (Supplementary Figure S1C, Luc-K12-3HA-4-*ofs*). Enhanced pre-

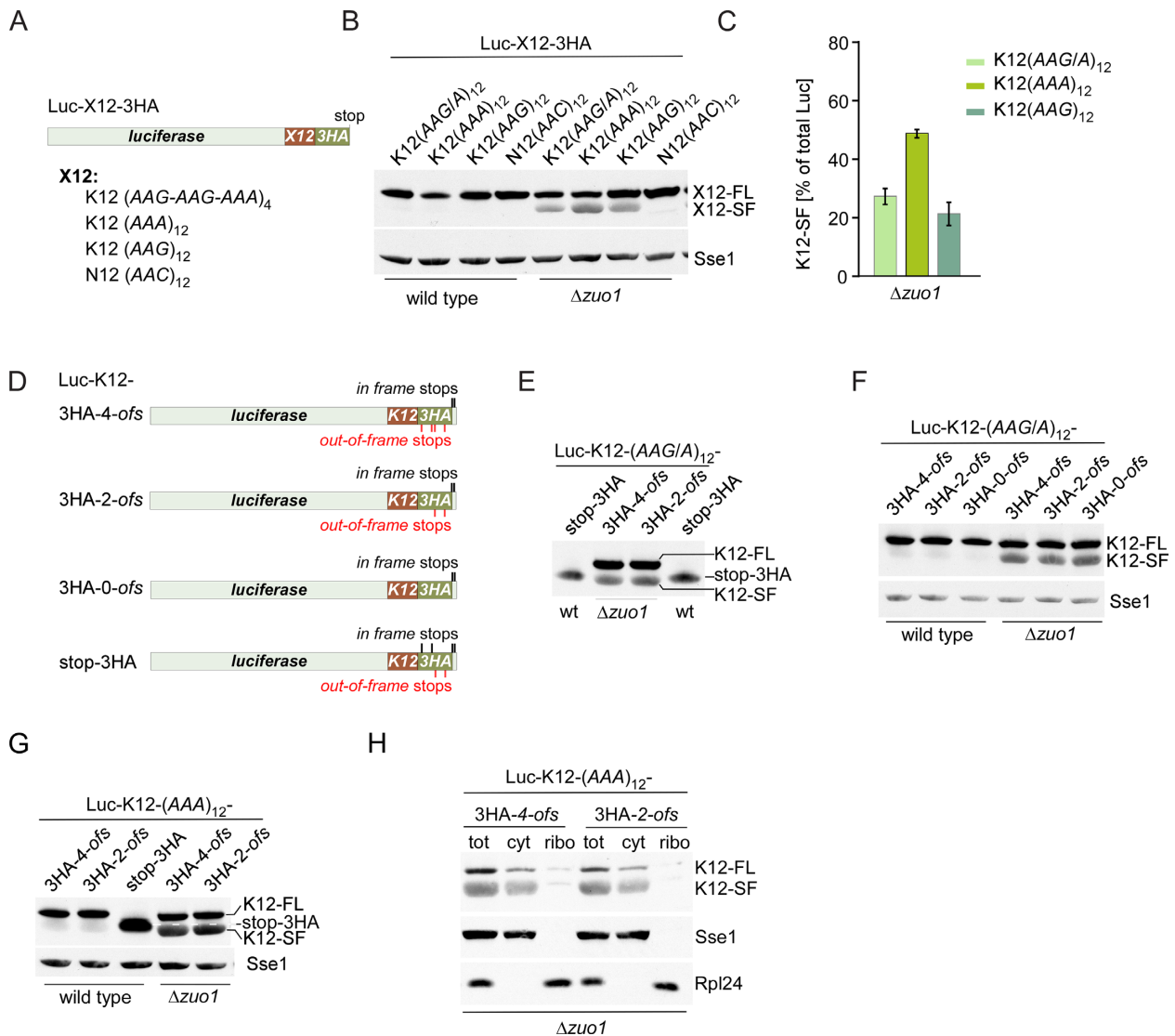


Figure 1. Premature translation termination in strains lacking RAC/Ssb occurs within the poly-AAG/A sequence. **(A)** Schematic representation of reporter constructs used for *in vivo* analysis of poly-AAG/A-stalling. **(B)** Expression of Luc-K12-3HA, with K12 segments encoded by poly-AAG/A sequences as indicated, in wild-type and $\Delta zuo1$ strains. Expression of Luc-N12-3HA served as a control. Total protein extracts were analyzed by immunoblotting using α -Luc for the detection of the full length (X12-FL) and shortened forms (X12-SF) and α -Sse1 as a loading control. **(C)** Quantitative analysis of the data shown in B. The relative amount of K12-SF is displayed as % of the total (K12-SF + K12-FL). Shown are means with SEM of at least four independent experiments (see ‘Materials and Methods’ section). **(D)** Schematic representation of the reporter constructs containing the indicated *in frame* and *out-of-frame* stop codons within the sequence encoding for the 3HA tag (see also Supplementary Figure S1C). **(E–G)** Expression of Luc-K12-3HA reporters containing different numbers of *out-of-frame* stop codons. Luc-K12-stop-3HA (Supplementary Figure S1C) indicates migration of a translation product (stop-3HA) lacking the 3HA tag. Translation products migrating faster than stop-3HA are truncated within the K12 segment. Analysis was performed as described in B. **(H)** C-terminally truncated translation products are efficiently released to the cytosol. Ribosome sedimentation assays of cell extracts from $\Delta zuo1$ strains expressing either Luc-K12(AAA)₁₂-3HA-4-ofs or Luc-K12(AAA)₁₂-3HA-2-ofs. Total cell extract (tot), cytosol (cyt) and ribosomal pellet (ribo) were prepared by centrifugation through a high-salt sucrose cushion (800 mM KOAc). Analysis was performed as described in B; α -Sse1 served as a cytosolic marker and α -Rpl24 as a ribosomal marker.

mature termination during translation of Luc-K12-3HA-4-ofs could thus result from ribosome sliding into a different *reading frame* (31) (Supplementary Figure S1B). If such an event took place during translation of the Luc-K12(AAG/A)-3HA-4-ofs reporter (termed Luc-K12-3HA in our previous study, 8), the first sliding-induced canonical termination event could occur two codons downstream of the (AAG-AAG-AAA)₄ sequence (Figure 1D and Supplementary Figure S1C). To test for this possibility, we gen-

erated two additional Luc-K12-3HA reporters (Figure 1D and Supplementary Figure S1C). In one, an *in frame TAG* stop codon was introduced so that canonical termination generates a translation product (termed stop-3HA) containing the full K12 segment plus two residues (Supplementary Figure S1C, Luc-K12-stop-3HA). In the other, the two most 5' situated *ofs* were removed by silent mutations (Supplementary Figure S1C, Luc-K12-3HA-2-ofs). If sliding occurred on Luc-K12-3HA-2-ofs, the first possible ter-

mination event would lead to a product containing K12 plus 20 additional residues, which would be clearly separable from stop-3HA via SDS-PAGE (Supplementary Figure S1C). Side by side analysis revealed that i) expression of Luc-K12-3HA-4-*ofs* and Luc-K12-3HA-2-*ofs* gave rise to exactly co-migrating K12-SF species (Figure 1E); ii) stop-3HA migrated more slowly when compared to K12-SF, indicating that translation termination on the Luc-K12-3HA-4-*ofs* and Luc-K12-3HA-2-*ofs* reporters in the $\Delta zuo1$ strain had occurred within the poly-*AAG/A* sequence (Figure 1E); and iii) K12-SF was produced even when the 3HA sequence of the reporter did not contain any *out-of-frame* stop codons (Figure 1F and Supplementary Figure S1C, Luc-K12-3HA-0-*ofs*). Because sliding is most efficient on polyA sequences (31,51,52) we also compared expression of Luc-K12(*AAA*)₁₂-3HA-4-*ofs* and Luc-K12(*AAA*)₁₂-3HA-2-*ofs* in $\Delta zuo1$ cells (Figure 1D and Supplementary Figure S1C). The resulting K12-SF products exactly co-migrated (Figure 1G). Furthermore, migration of K12-SF indicated that the C-terminally truncated polypeptides were smaller than stop-3HA, indicating that termination had occurred within the (*AAA*)₁₂ sequence (Figure 1G). K12-SF with (*AAA*)₁₂-encoded K12 was efficiently released from ribosomes (Figure 1H), which resembles previous observations with (*AAG-AAG-AAA*)₄-encoded K12-SF (8). The combined data confirm that in cells lacking the RAC/Ssb system, premature nascent polypeptide release occurs due to a non-canonical termination event when ribosomes translate poly-*AAG/A* sequences.

Ribosome stalling and stop codon readthrough is enhanced in the absence of a functional RAC/Ssb system *in vitro*

We next employed a homologous *in vitro* translation system to obtain mechanistic insight into the role of RAC/Ssb with respect to premature nascent polypeptide release and readthrough. For these experiments translation extracts were prepared from wild-type or a $\Delta zuo1$ strain, in which the RAC/Ssb system is non-functional, even though Ssb is still present (13,14). Initial experiments were performed with the mHis3-K20-3HA-ws reporter (Figure 2A), which is an *in frame* fusion of *HIS3*, a poly-*AAG/A* sequence encoding for 20 consecutive lysine residues (K20, Supplementary Figure S2A), a sequence encoding for a 3HA tag, and a weak stop codon (ws, Supplementary Figure S2B). This reporter enabled us to analyze ribosome stalling on poly-*AAG/A* and stop codon readthrough in a single translation reaction. mHis3-ss (Figure 2A and Supplementary Figure S2B), which is free of stalling sequences and contains a strong stop codon (ss) at the end of the *HIS3 orf*, was employed as a control. As expected, *in vitro* translation of the mHis3-ss transcript gave rise to a single translation product of ~24 kDa, which corresponds to the mass of the full length His3 protein (His3-FL) (Figure 2B). Translation of mHis3-ss followed similar kinetics in wild-type and $\Delta zuo1$ extracts, indicating that *in vitro* translation was not significantly impaired in absence of RAC/Ssb (Figure 2B, His3-FL). Translation of mHis3-K20-3HA-ws in wild-type extract gave rise to two major translation products (Figure 2B, upper panel). One, termed the stalled form K20-SF, migrated slightly above His3-FL indicating that trans-

lation had come to a halt shortly 3' of the *HIS3 orf*, within the poly-*AAG/A* stalling sequence. The other, termed K20-FL, corresponded to full length His3-K20-3HA (Figure 2B, upper panel). Stalled K20-SF was detected after about 10 min of translation, was maximally expressed after 30–40 min, and disappeared at later time points at the expense of K20-FL, which increased steadily (Figure 2B, upper panel). Upon translation of His3-K20-3HA-ws in $\Delta zuo1$ extract, the amount of stalled K20-SF was increased and the appearance of full length K20-FL was further delayed when compared to the wild-type (Figure 2B, lower panel). In addition, in the $\Delta zuo1$ extract a species migrating above K20-FL was detected at later time points. This species, corresponded in size to the readthrough translation product (K20-RT, Figure 2A) carrying a C-terminal extension of 36-residues due to readthrough of the first termination codon and termination at the second *in frame* stop codon (Figure 2B, lower panel and Supplementary Figure S2C). Readthrough was prevented when translation was performed with the mHis3-K20-3HA-ss reporter (Figure 2A and Supplementary Figure S2B), which contains a strong stop codon (Figure 2C, $\Delta zuo1$ ss), or with the mHis3-K20-3HA-4s reporter (Figure 2A and Supplementary Figure S2B), which contains four stops, two in *frame* plus one each in the –1 and +1 *frames* (Figure 2C, $\Delta zuo1$ 4s). *Vice versa*, when the strong stop codon at the end of the *HIS3 orf* was exchanged for a weak stop codon (Figure 2A and Supplementary Figure S2B), efficient readthrough occurred in $\Delta zuo1$, while in the wild-type readthrough remained low and the His3-RT band was hardly visible (Figure 2D and Supplementary Figure S2D). The combined data confirm previous observations indicating that the absence of RAC/Ssb causes a strong, stop codon-dependent, stimulation of readthrough (Figure 2B–D) (28).

To study translational stalling in more detail we employed His3-K20-3HA-ss (Figure 2A), in which stalling occurred, but stop-codon readthrough did not (Figure 2C). Upon translation of His3-K20-3HA-ss, K20-SF accumulated temporarily, however, after a delay was converted to the full length K20-FL product. When functional RAC/Ssb was absent from the translation reaction, the delay was more pronounced and a smaller fraction of stalled K20-SF was converted to full length K20-FL (Figure 2E). Accumulation of the intermediate (Figure 2B and E) suggested that K20-SF remained ribosome-bound and was completed to full length K20-FL with a delay. To test this directly, we separated translation reactions primed with mHis3-K20-3HA-ss on Bis-Tris gels, on which peptidyl-tRNA bonds remain intact. While K20-FL was released from ribosomes, the bulk of K20-SF remained bound as peptidyl-tRNA, which was readily cleaved by RNase A treatment (Figure 2F). Consistent with the more pronounced accumulation of K20-SF in the $\Delta zuo1$ extract (Figure 2B and E), more K20-SF was attached to tRNA in the absence of functional RAC/Ssb. The amount of peptidyl-tRNA bound to ribosomes in the $\Delta zuo1$ translation reaction was reduced when purified RAC (Supplementary Figure S3A) was added prior to the translation reaction. We conclude that ribosomes stalled during translation of poly-*AAG/A* *in vitro* were stable and no, or only little, peptide release occurred, even

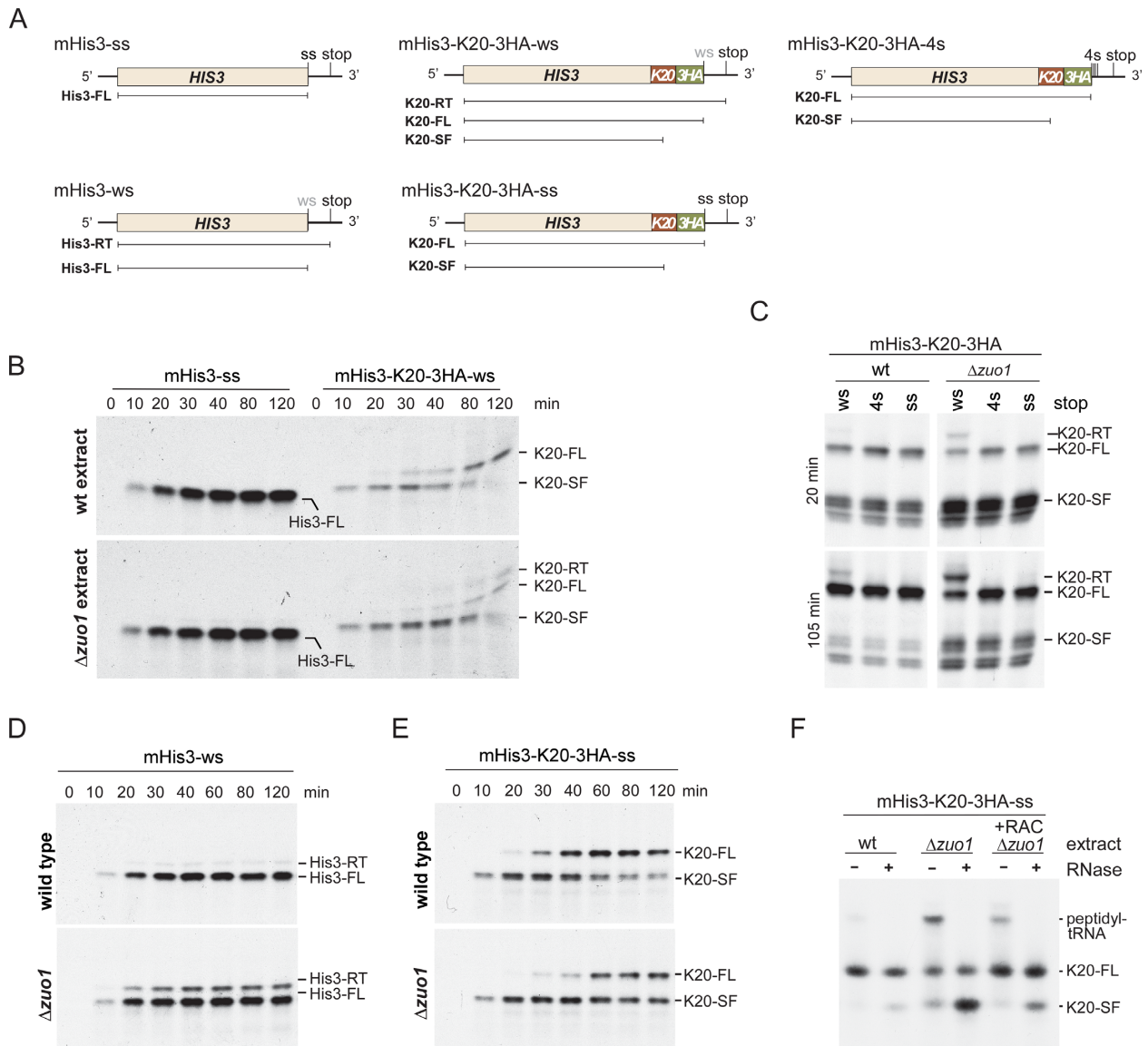


Figure 2. The absence of RAC/Ssb induces stop codon readthrough and enhances ribosome stalling on poly-AAG/A sequences *in vitro*. (A) Schematic representation of reporter transcripts and the corresponding translation products. mHis3: mRNAs containing the *HIS3* coding sequence; K20: poly-AAG/A sequence encoding for 20 consecutive lysine residues (Supplementary Figure S2A); 3HA: sequence encoding for the 3HA tag (Supplementary Figure S1C); ss: strong stop codon context (Supplementary Figure S2B); ws: weak stop codon context (Supplementary Figure S2B); full length translation products (FL), stalled forms (SF), readthrough products (RT). (B) Enhanced readthrough and stalling on poly-AAG/A in the absence of RAC/Ssb. Translation time courses of the indicated transcripts was performed in wild-type or Δ zuo1 translation extract in the presence of [³⁵S]-methionine at 20°C for the times indicated. Subsequently, aliquots of the reactions were separated on 12% Tris-Tricine gels and were analyzed via autoradiography. (C) Stop codon readthrough depends on the stop codon and context. *In vitro* translation of the indicated transcripts in wild-type and Δ zuo1 extracts was performed for 20 and 105 min at 20°C and translation products were analyzed via autoradiography. (D and E) Translation time courses of the readthrough reporter mHis3-ws (D) and the stalling reporter mHis3-K20-3HA-ss (E) in wild-type and Δ zuo1 translation extracts. (F) K20-SF is bound to ribosomes as a peptidyl tRNA in Δ zuo1 translation extract. Peptidyl-tRNAs generated via *in vitro* translation of the stalling reporter mHis3-K20-3HA-ss were analyzed on Bis-Tris gels. If indicated purified RAC (Supplementary Figure S3A, 49 pmol/20 μ l) was added to the translation reaction prior to the addition of mRNA. RNaseA was added (+ RNase) to digest the peptidyl-tRNA bond.

in the absence of RAC/Ssb. This differs from the situation in living cells lacking RAC/Ssb (Figure 1), where stalled translation products are released as C-terminally truncated translation products, rather than accumulating as ribosome-bound peptidyl tRNAs (8). The reason as to why nascent chain release does not occur *in vitro* remains unclear. One possible explanation is the general inability

of the yeast-derived *in vitro* translation system to promote ubiquitination reactions e.g. via E3 ubiquitin ligases. Yet *in vivo*, the E3 ubiquitin ligase Hel2 is required for premature nascent polypeptide release in the absence of RAC/Ssb (Supplementary Figure S3B and Explanatory Text Supplementary Figure S3B).

Addition of RAC to $\Delta zuo1$ translation extract rescues ribosome stalling, but does not rescue stop codon readthrough

The impact of RAC/Ssb on translation fidelity could be direct, because RAC/Ssb impacts on the decoding process (14,28,29,53), or indirect, as for example, because ribosomes do not properly assemble when RAC/Ssb is absent (19,23,24). If the role of RAC/Ssb was direct, addition of RAC to $\Delta zuo1$ translation extract should rescue stalling and readthrough defects described above (Figure 2). Conversely, if translational errors in the absence of RAC/Ssb were due to improper ribosome assembly, addition of RAC to $\Delta zuo1$ translation extract should have no impact. To distinguish between these possibilities, we added purified RAC (Supplementary Figure S3A) to wild-type or $\Delta zuo1$ translation extract prior to addition of reporter mRNA. RAC addition did not affect translation reactions primed with mHis3-ss control reporter (Supplementary Figure S3C). However, when RAC was added to the $\Delta zuo1$ extract, translation products derived from the stalling/readthrough reporter mHis3-K20-3HA-ws (Figure 2A) changed in an unexpected manner. Upon addition of RAC to the $\Delta zuo1$ extract, expression of stalled K12-SF was reduced to the level observed in wild-type extract; however, in the same experiment, expression of the readthrough product K20-RT remained high (Figure 3A–C). This observation suggested that stalling, but not readthrough, was due to a direct effect of the RAC/Ssb system.

We previously found that paromomycin strongly enhances stop codon readthrough in the absence of functional RAC/Ssb *in vivo* and *in vitro* (28). We now employed this observation to corroborate the distinct effects of RAC/Ssb with respect to stalling and readthrough, employing mHis3-ws as a readthrough reporter, and His3-K20-3HA-ss as a stalling reporter (Figure 2A). Upon translation in wild-type extract, paromomycin neither induced readthrough (Figure 3D, upper panel), nor stalling (Figure 3D, lower panel). This is consistent with the notion that paromomycin does not bind to the decoding center of the yeast ribosome (27). In the absence of functional RAC/Ssb, however, paromomycin strongly enhanced readthrough (His3-RT, Figure 3D, upper panel) and also enhanced stalling, such that the production of full length product was nearly abolished (K12-FL, Figure 3D, lower panel). Purified RAC added to $\Delta zuo1$ extract prevented paromomycin-induced stalling, however, did not affect paromomycin-induced stop codon readthrough (Figure 3D, upper and lower panel $\Delta zuo1$ + RAC). Thus, whilst the addition of RAC was able to rescue stalling of ribosomes on poly-AAG/A, addition of RAC did not prevent readthrough of a weak stop codon. Based on the combined data we conclude that RAC plays a direct role in ribosome stalling on poly-AAG/A sequences. However, the role of RAC/Ssb in stop codon readthrough was seemingly more indirect.

To determine the position of stalled ribosomes on the reporter mRNA, we employed the method of primer extension by reverse transcriptase (41). To this end, we constructed a short stalling reporter mGlk1-K20-2HA-ss suited for primer extension analysis, which consists of the first 120 bases of *GLK1*, the poly-AAG/A sequence, a sequence encoding for a 2HA tag and a strong stop

codon (Figure 4A and Supplementary Figure S4A). As a readthrough reporter we employed mGlk1-stop-K20-2HA-ss, which resembles mGlk1-K20-2HA-ss, however, contains a TAA *in frame* stop codon at the end of the *GLK1-120* sequence (Figure 4B and Supplementary Figure S4A). Proper formation of toeprints was tested by adding cycloheximide prior to the translation reactions. As expected the addition of cycloheximide resulted in a single, strong toeprint +16 nucleotides downstream the ATG (A = +1), indicating that ribosomes had stalled with the initiation codon in the A-site (Figure 4C and D, lanes + CHX) (54,55,56). Toeprint analysis with mGlk1-K20-2HA-ss revealed that stalling of ribosomes occurred mainly within the poly-AAG/A sequence of the reporter. The reason for ribosome stalling 5' of the poly-AAG/A sequence in the wild-type is unclear (Figure 4C, toeprints indicated by black asterisks). Possibly, methionyl-tRNA was limiting in the *in vitro* system and thus the multiple AUG codons 5' of the poly-AAG/A (Supplementary Figure S4A) behaved as 'hungry codons' leading to ribosome pausing (57,58). In any case, the pattern of toeprints within the poly-AAG/A region in wild-type or $\Delta zuo1$ extracts was similar: stalling occurred already at the first lysine codon, reached a maximum between lysine codons 7 and 11, and decreased along the remainder of the sequence (Figure 4C, toeprints +13, +31, +34, +40 and +43 and Figure 4E). Importantly, the toeprints observed upon translation in the $\Delta zuo1$ extract were strongly enhanced when compared to the wild-type and were returned to the wild-type level when RAC was added prior to the translation reaction (Figure 4C, toeprints +13, +31, +34, +40 and +43). The data are consistent with a model in that stalling on poly-AAG/A is enhanced in the absence of functional RAC/Ssb and this effect is connected to a direct function of RAC/Ssb in the translation process.

Toeprinting with mGlk1-stop-K20-2HA-ss (Figure 4B and Supplementary Figure S4A) in wild-type translation extract did not reveal significant signals downstream of the UAA stop codon (Figure 4D). A weak toeprint +13 nucleotides of the UAA codon indicated that a minor fraction of ribosomes was pausing at the stop codon prior to termination (Figure 4D and F, toeprint +13) (55). This +13 toeprint was strongly enhanced in the absence of RAC/Ssb, indicating that ribosomes paused more frequently, or for a prolonged period of time, at a stop codon in the absence of RAC/Ssb. This behavior was not due to a reduced concentration of eRF1/eRF3 in the $\Delta zuo1$ translation extract (Supplementary Figure S4B). Addition of purified RAC to $\Delta zuo1$ extract prior to translation did not reduce the +13 toeprint (Figure 4D). We conclude that in the absence of a functional RAC/Ssb system, ribosomes pause at stop codons and this effect is not connected to a direct function of RAC/Ssb in translation.

Ribosomes assembled in cells lacking RAC/Ssb display high affinity for paromomycin

Previous studies revealed that the IC₅₀ values, by which distinct aminoglycosides inhibit eukaryotic translation, correlate with their affinities for the h44 decoding region (59,60). Based on the above data we speculated that ribosomes from cells lacking RAC/Ssb might display enhanced affinity for

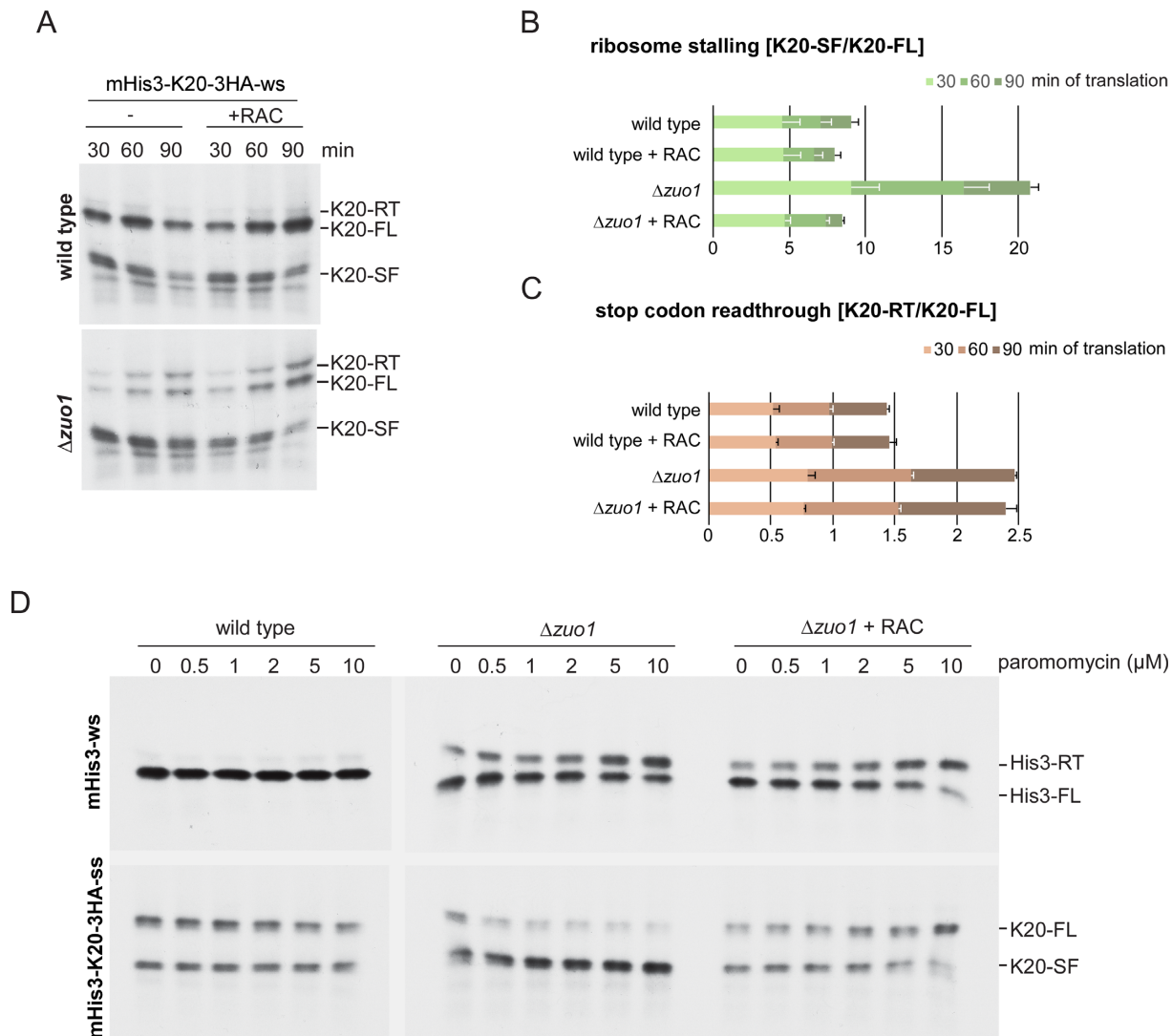


Figure 3. Complementation of $\Delta zuo1$ translation extract with purified RAC prevents stalling on poly-*AAG/A* but does not prevent stop codon readthrough. (A) RAC affects *in vitro* translation of poly-*AAG/A* in $\Delta zuo1$ translation extract. If indicated, purified RAC (Supplementary Figure S3A, 49 pmol/20 μ l) was added to wild-type or $\Delta zuo1$ translation extract prior to addition of mHis3-K20-3HA-ws. Translation reactions were performed and analyzed as described in Figure 2B. (B and C) Quantitative analysis of the data shown in A and Supplementary Figure S3D. K20-SF, K20-FL and K20-RT were quantified using AIDA Image Analysis software. Shown is the ratio of K20-SF/K20-FL (B) and K20-RT/K20-FL (C), respectively. Error bars indicate the SEM of three independent experiments. (D) Purified RAC does not affect *in vitro* stop codon readthrough in $\Delta zuo1$ translation extract. Translation reactions were performed with the readthrough reporter mHis3-ws and the stalling reporter mHis3-K20-3HA-ss in wild-type and $\Delta zuo1$ extracts complemented with RAC for 50 min at 20°C as described in A. Paromomycin was added to the translation reactions at the concentrations indicated.

paromomycin when compared to the wild-type. To test this directly, we analyzed the binding affinity of ribosomes purified from either wild-type or from a yeast strain lacking RAC/Ssb (termed ribosomes $_{\Delta RAC/Ssb}$ -assembled) for paromomycin via ITC (Figure 5 and Supplementary Figure S5). To that end, ribosomes were purified under high-salt conditions removing RAC and Ssb from core ribosomal particles (Figure 5A) (33,61). Purified ribosomes from cells lacking RAC/Ssb displayed high affinity paromomycin binding (Figure 5B and Supplementary Figure S5, $K_D = 76.6$ nM). Consistent with previous observations (3,27), and with the data presented above (Figure 3D), wild-type ribosomes displayed low affinity for paromomycin such that under the experimental conditions binding was below the detection

limit (Figure 5C). The observation strongly suggested that ribosomes $_{\Delta RAC/Ssb}$ -assembled differed in some structural aspect, which led to enhanced affinity for paromomycin and reduced translational fidelity.

Ribosomes assembled in cells lacking RAC/Ssb display structural alterations at the decoding and peptidyl transferase centers

The fidelity of translation depends on the precise structural features of the rRNA, which are established in a highly orchestrated process involving pre-rRNA processing and folding, introduction of rRNA modifications and proper assembly with ribosomal proteins (1,2,62). Most abundant rRNA modifications are pseudouridylation and 2'-O-methylation,

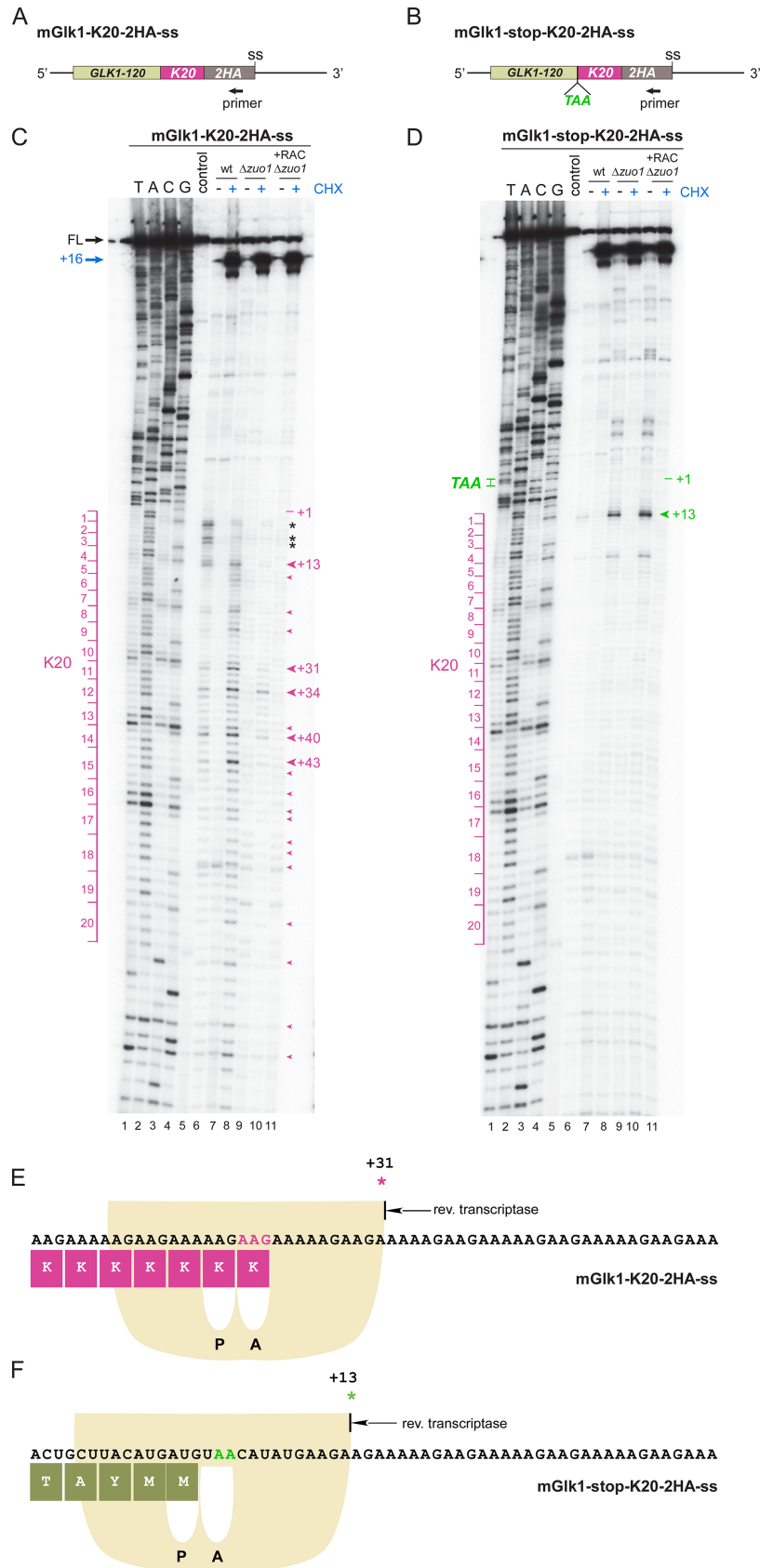


Figure 4. Toeprint analysis of ribosome stalling on poly-AAG/A and the UAA stop codon. (A and B) Schematic representation of reporters employed for toeprint analysis. The sequence of the transcript and translation product is shown in Supplementary Figure S4A. The TAA codon is shown in green.

which occur in functionally important regions, such as the decoding center, the PTC and the ribosomal tunnel (2,62,63). A number of mutants with defects in such modifications display decreased translational fidelity and altered sensitivity toward paromomycin and other translational inhibitors (58,64,65,66). Indeed, in some cases the loss of base modification leads to minor structural changes of the rRNA within regions important for the maintenance of translation fidelity (64,65). We therefore employed dimethyl sulfate (DMS) chemical probing to test if structural alterations were detectable within h44 of the 18S rRNA (Figure 6A and B; Supplementary Figure S6A) and/or the PTC of the 25S rRNA (Figure 6C and D; Supplementary Figure S6B) of ribosomes $_{\Delta RAC/Ssb}$ -assembled.

A comparison with wild-type ribosomes revealed that DMS modification of G1638 was strongly enhanced in ribosomes $_{\Delta RAC/Ssb}$ -assembled (Figure 6A). Of note, the nucleotide adjacent to G1638, C1639, is 2'-O-methylated, and loss of C1639 2'-O-methylation affects translational fidelity and paromomycin sensitivity (58,67,68). In addition, ribosomes $_{\Delta RAC/Ssb}$ -assembled displayed enhanced modification of nucleotides A2801, A2802 (E-site), A2803 (E-site), G2805, G2815, G2816, A2819, C2821 (P-site) and G2831 (Figure 6C–E). Thus, specific nucleotides, intimately connected to the decoding process, were de-protected toward DMS-modification in ribosomes $_{\Delta RAC/Ssb}$ -assembled. The data indicate that ribosomes assembled in cells lacking RAC/Ssb suffer from subtle conformational changes within the decoding center, which provide an explanation for enhanced paromomycin binding (Figure 5) and reduced fidelity of translation termination (Figures 1–4).

DISCUSSION

Ribosomes assembled in the absence of RAC/Ssb differ structurally from ribosomes assembled in wild-type cells

In this work we uncover differences between ribosomes assembled in wild-type cells and ribosomes assembled in cells lacking a functional RAC/Ssb system. Ribosomes $_{\Delta RAC/Ssb}$ -assembled displayed strongly enhanced affinity for paromomycin. As binding affinities were compared with RAC/Ssb-free ribosome preparations this was not due to a direct effect of RAC/Ssb. Rather, structural alterations at the ribosomal decoding center and the PTC suggest that paromomycin can interact with h44 of ribosomes $_{\Delta RAC/Ssb}$ -assembled. Such a model is supported by the observation that enhanced affinity of

ribosomes $_{\Delta RAC/Ssb}$ -assembled for paromomycin correlates with the effect of the drug on translational fidelity *in vitro* and *in vivo*, as well as with paromomycin hyper-sensitivity of yeast cells lacking RAC/Ssb.

The most critical region of the ribosome with respect to paromomycin binding is h44 at the decoding center. Even a single nucleotide exchange within h44 can switch a ribosome from paromomycin 'sensitive' to 'resistant' (3,59,60). Wild-type ribosomes and ribosomes $_{\Delta RAC/Ssb}$ -assembled possess identical rRNA sequences. Thus, a possible explanation for the above observations is that wild-type ribosomes and ribosomes $_{\Delta RAC/Ssb}$ -assembled differ with respect to covalent rRNA modifications, allowing for more efficient accommodation of near-cognate tRNAs in ribosomes $_{\Delta RAC/Ssb}$ -assembled. This model is supported by de-protection of critical nucleotides of the rRNA of ribosomes $_{\Delta RAC/Ssb}$ -assembled (see 'Results' section). Consistently, it was reported that rRNA modifications can affect paromomycin binding, translational fidelity, and *in vivo* sensitivity towards the drug (64,65,68). An interesting case is the eukaryotic organism *Leishmania*, which is exceptional because h44 of the *Leishmania* 18S rRNA interacts with paromomycin and *Leishmania* is paromomycin sensitive (69) (Supplementary Figure S7A–D). At first glance this is surprising, because critical nucleotides of *Leishmania* h44 resemble those of other eukaryotic organisms, which do not interact with paromomycin (Supplementary Figure S7A–C). However, the rRNA modification pattern of the *Leishmania* decoding center differs from other eukaryotes, and in fact, more closely resembles the decoding centers of paromomycin sensitive bacterial species (69). Also noteworthy is the connection between Ssb and snoRNA snR18, which guides 2'-O-methylation of two adjacent 25S rRNA nucleotides exposed to the exit tunnel. A genetic screen identified Ssb and snR18 as the most effective multicopy enhancers of translation termination fidelity (70).

Future experiments will need to establish by exactly what mechanism the loss of RAC/Ssb leads to the subtle structural changes, which impact on paromomycin binding and translational fidelity. In the nucleolus RAC/Ssb may be involved in keeping pre-rRNAs in accessible conformations to allow for the base-pairing of snoRNAs and binding of associated factors (1,2,62). Such, in a broader sense, chaperone-type of action may not only provide an explanation for altered covalent modifications within the rRNA but also for the observed pre-rRNA processing defects in cells lacking RAC/Ssb (19). Interestingly, loss of rRNA modifi-

The position of the primer used for primer extension in toeprint experiments is indicated by the black arrow. (C and D) Toeprint analysis of the stalling reporter mG1k-K20-2HA-ss (C) and the readthrough reporter mG1k-stop-K20-2HA-ss (D). Translation reactions were performed in wild-type or $\Delta zuo1$ extract for 90 min at 20°C in the presence (+) or absence (–) of 300 μ g/ml cycloheximide (CHX). If indicated purified RAC was added prior to the translation reaction as described in Figure 3. Primer extension was subsequently performed with ribosomal complexes collected by centrifugation as described in 'Materials and Methods' section. The control lane corresponds to a reaction without translation extract. Samples were separated on 7.5% urea-polyacrylamide gels together with the appropriate sequencing ladder (lanes 1–4). The full length extension product (FL) is indicated by the black arrow and the product corresponding to cycloheximide-stalled initiation complexes (16 nucleotides downstream of the AUG initiation codon) is indicated by the blue arrow (+16). The K20 sequence AAG-AAA-(AAG-AAG-AAA)₆ is indicated by the pink ladder. The TAA stop codon of mG1k-stop-K20-2HA-ss is indicated in green. Colored arrows represent stops of the reverse transcriptase (toeprints) due to stalling of ribosomes on the K20 sequence (pink), or on the UAA stop codon (green). The position of the main toeprints are numbered relative to the first lysine codon of mG1k-K20-2HA-ss (C) and relative to the UAA stop codon of mG1k-stop-K20-2HA-ss (D). The black asterisks indicate toeprints due to ribosome stalling upstream of the K20 sequence. (E and F) Schematic representation of the toeprint results. Shown is the ribosome stalled with codon 7 (AAG) of the poly-AAG/A in the A-site (E) or with the UAA stop codon in the A-site (F). These ribosome stalls result in toeprints at +31 (relative to the first nucleotide of the first lysine codon) and position +13 (relative to the first nucleotide of the UAA), respectively.

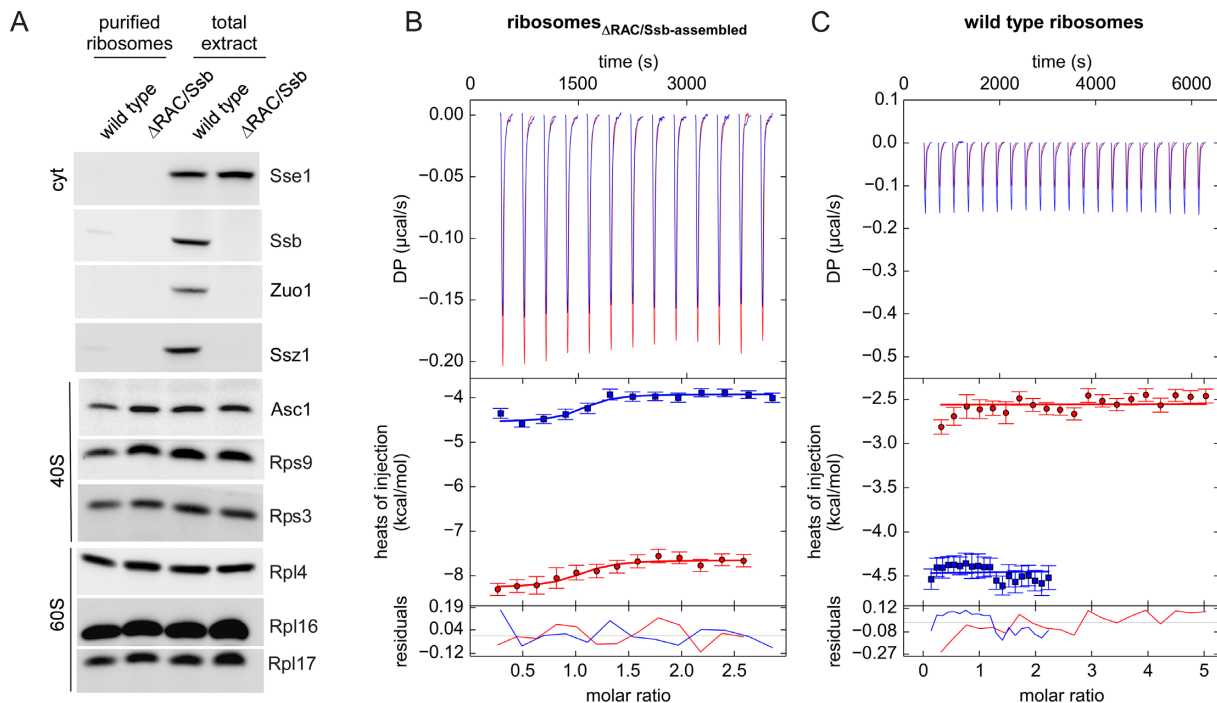


Figure 5. Paromomycin binds to ribosomes Δ RAC/Ssb-assembled with high affinity. (A) Immunoblot analysis of purified wild-type ribosomes and ribosomes Δ RAC/Ssb-assembled employed for the ITC experiment. In comparison, total cell extract of the wild-type and the Δ RAC/Ssb strains. Samples were separated on 10% Tris-Tricine gels and were analyzed via immunoblotting using α -Sse1 (cyt: cytosolic marker), α -Ssb1, α -Zuo1, α -Ssz1 (RAC/Ssb chaperone triad), α -Asc1, α -Rps9, α -Rps3 (40S ribosomal proteins), α -Rpl4, α -Rpl16, α -Rpl17 (60S ribosomal proteins). (B and C) ITC recording. Singular value decomposition (SVD) reconstructed thermograms (upper panel), fits and derived thermodynamic binding parameters (middle panel) and residuals plots for the fits (lower panel) of the paromomycin interaction with ribosomes Δ RAC/Ssb-assembled (B) or wild-type ribosomes (C) (for details see 'Materials and Methods' section).

cations in the decoding center impairs pre-rRNA processing (71). Alternatively, RAC/Ssb may act as a chaperone during other steps of ribosome biogenesis. Several ribosomal proteins affect paromomycin binding and translational fidelity (3,72,73). If RAC/Ssb was required for proper assembly, or post-translational modification of one or more ribosomal proteins, this may account for enhanced paromomycin binding and reduced translational fidelity in the absence of RAC/Ssb. RAC/Ssb may also impact on ribosome biogenesis via its role in TORC1-dependent signaling (24,74) (see also Introduction). Some snoRNA-mediated rRNA modifications are regulated in a TORC1-dependent manner (75,76) and, via its regulation of Pol III, TORC1 regulates expression of 5S rRNA, which transmits and coordinates the function of the decoding center and PTC (77). These different possibilities are not mutually exclusive and it is tempting to speculate that RAC/Ssb exerts a combined effect on more than one aspect of ribosome biogenesis.

RAC/Ssb affects stop codon recognition, but does not affect ribosome sliding

A recent study suggested that C-terminally truncated polypeptides generated upon translation of poly-*AAG/A* in strains lacking RAC/Ssb might result from enhanced ribosome sliding followed by canonical termination at *out-of-frame* stop codons (31). The data presented here reveal that this is not the case. First, release of C-terminally truncated

polypeptides was observed when the polylysine segment of the reporter was encoded by (*AAG*)₁₂, a sequence which does not induce ribosome sliding (31); second, C-terminally truncated polypeptides were smaller in size than a control protein that mimicked the product of ribosome sliding; third, and most importantly, the production of C-terminally truncated polypeptides was also detected when the complete set of possible *out-of-frame* stop codons was removed from the sequence downstream of the poly-*AAG/A*.

How then does premature release of truncated polypeptides occur in the absence of RAC/Ssb? We propose that the structural changes described above play a pivotal role in this unconventional termination process. Binding of eRF1/eRF3 to the mammalian A-site involves 'flipping' of A1825 within h44 of rabbit ribosomes (6). This base corresponds to *Leishmania* A2159 (Supplementary Figure S7B), which is 'flipped' in the paromomycin-bound structure (69) (Supplementary Figure S7D). The strongly enhanced binding affinity of ribosomes Δ RAC/Ssb-assembled to paromomycin suggests that 'flipping' of the corresponding adenosine (A1756 in *Saccharomyces*, Supplementary Figure S7A) is facilitated. This situation likely becomes relevant when ribosomes Δ RAC/Ssb-assembled slow down during the translation of poly-*AAG/A* sequences (see also below). During the termination process the eukaryotic ribosomal A-site accommodates four instead of three nucleotides, decoding +2 and +3 as a unit, allowing for only *AA*, *AG* and *GA*, but not *GG* (6). Of note, both lysine codons (*AAA* and

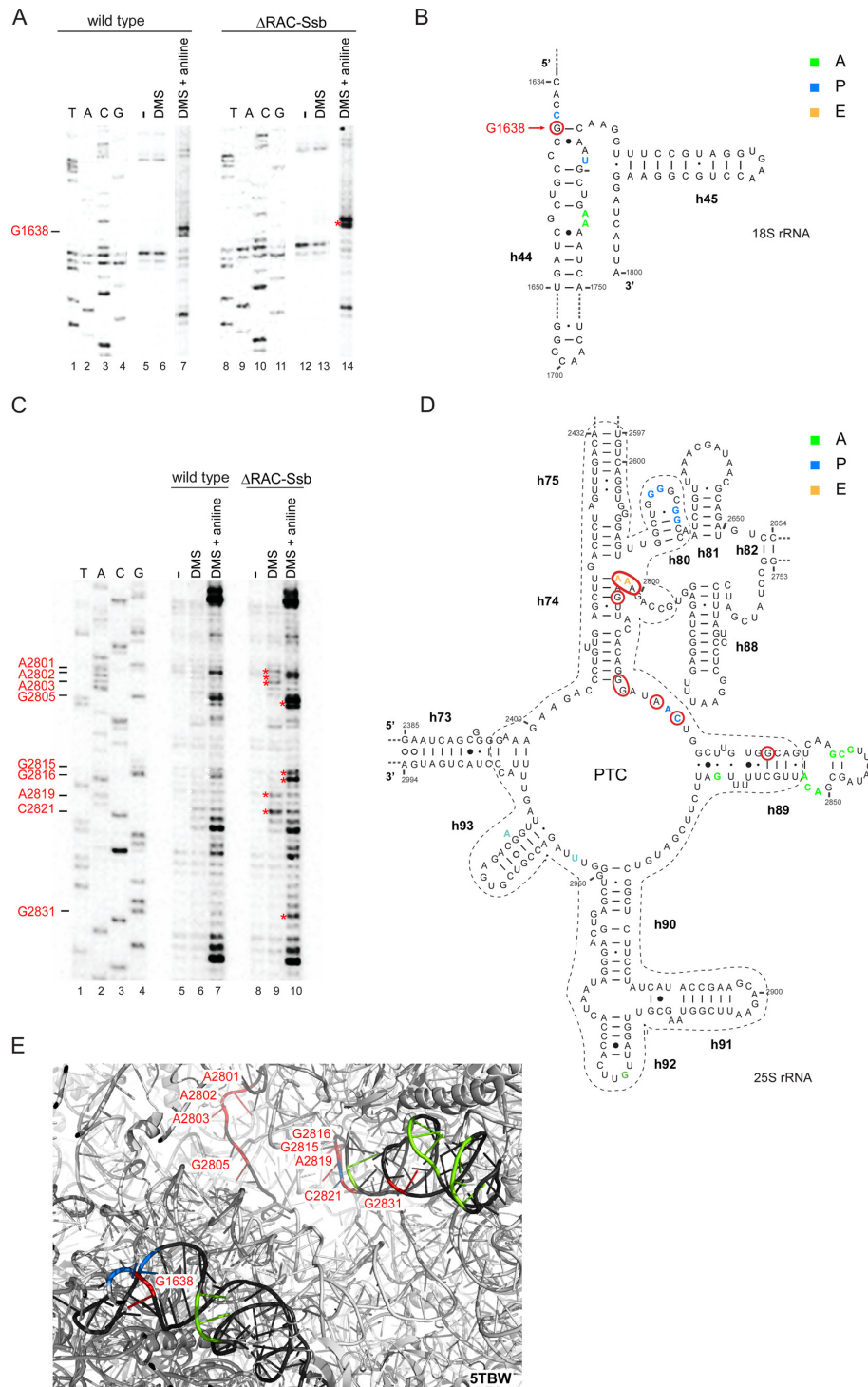


Figure 6. Chemical probing of the rRNA structure at the decoding center and PTC of wild-type and ribosomes Δ RAC/Ssb-assembled. **(A)** DMS chemical probing of h44 of the 18S rRNA in wild-type ribosomes (lanes 5–7) or ribosomes Δ RAC/Ssb-assembled (lanes 12–14). DMS methylated N1 of adenosine and N3 of cytosine block reverse transcriptase, which can be directly detected via primer extension (DMS). Methylation at N7 of guanosine can be detected by primer extension analysis after reduction with NaBH₄ followed by aniline treatment (DMS + aniline). For details see ‘Materials and Methods’ section. Untreated samples are shown as a control (–). Reactions were performed in triplicate, representative autoradiographs are shown (see also Supplementary Figure S6A). Deprotected G1638, which migrates as a doublet after NaBH₄/aniline treatment, is labeled in red and marked by a red asterisk. **(B)** Secondary structure of yeast h44/h45 of the 18S rRNA with A-site bases (green), P-site bases (blue) and deprotected G1638 circled in red. **(C)** DMS chemical probing of the 25S rRNA PTC of wild-type ribosomes (lanes 5–7) or ribosomes Δ RAC/Ssb-assembled (lanes 8–10). The experiment was described as described in (A) (see also Supplementary Figure S6B). Deprotected bases are labeled in red and are marked by red asterisks. **(D)** Secondary structure of the yeast 25S rRNA at the PTC. Bases located in the A-, P- and E-sites are highlighted in green, blue and yellow, respectively. Nucleotides deprotected from DMS-methylation in ribosomes Δ RAC/Ssb-assembled are circled in red. **(E)** View of the *Saccharomyces cerevisiae* decoding center/PTC region with h44 and h89 in black, A-site bases (green) P-site bases (blue) and deprotected bases of ribosomes Δ RAC/Ssb-assembled (red) (PDB 5TBW).

for non-canonical nascent chain release. Such a difference between ribosomes stalled *in vivo* or *in vitro* is not without precedence. During translation of transcripts which entirely lack *in frame* stop codons (stop codon-less transcripts), ribosomes stall at the very end of the message, with the A-site empty. *In vivo* translation products derived from stop codon-less transcripts are efficiently released in a reaction that requires the eRF1/eRF3-homologs Dom34/Hbs1 (8,30,78). *In vitro*, however, translation products derived from stop codon-less transcripts remain ribosome-bound, leading to stable ribosome nascent chain complexes. Noteworthy, premature nascent polypeptide release in the absence of RAC/Ssb depends on the small ribosomal subunit protein Asc1 (8) and the E3 ubiquitin ligase Hel2 (Supplementary Figure S3B). Asc1 and Hel2 were recently shown to be required for the ubiquitination of a specific set of small subunit ribosomal proteins, which in turn is a requirement for the resolution of stalled ribosomes (79,80,81). As protein ubiquitination does not occur in the *in vitro* translation system employed in this study, this provides a possible explanation for the uncoupling of ribosome stalling from premature translation termination (see Supplementary Figure S3B Explanatory Text).

Enhanced ribosome stalling on poly-AAG/A is connected to a direct function of RAC/Ssb

Early studies in yeast suggested that stalling was mainly due to electrostatic interactions between positively charged nascent chain segments consisting of lysine or arginine residues and the negatively charged surface of the ribosomal exit tunnel (30,81,82,83). Later findings revealed that ribosome stalling is more complex and codon sequence and context play a significant role (30,31,51,84,85). Here we show that enhanced stalling on poly-AAG/A in strains lacking RAC/Ssb was codon dependent and occurred at the very 5'-end of a poly-AAG/A sequence, a situation which resembles previous observations in the *Escherichia coli* system (31). This finding excludes that the interaction of a polylysine segment with either the tunnel wall, or with RAC/Ssb is the major cause for ribosome stalling on poly-AAG/A. How then does RAC/Ssb affect ribosome stalling? Our data reveal that sequence-specific stalling was connected to a direct function of RAC/Ssb in the translation process. We propose that two functional properties of the RAC/Ssb system jointly promote translation of poly-AAG/A. First, Zuo1 forms an extended structure, which at one end carries a domain interacting with the 60S subunit close to the polypeptide tunnel exit (14,29,53,72) and, at the other end, carries a domain interacting with expansion segment 12 (ES12) at the tip of h44 (14,29) (Figure 7A). As discussed above, h44 is at the heart of the 40S decoding center. Thus, RAC—via the Zuo1 contact to ES12—may influence decoding. Second, the general speed of translation is reduced when Ssb does not interact with nascent chains (8,17) and the interaction of Ssb with nascent chains depends on RAC (13,15). Even though a RAC-free translation extract contains structurally altered ribosomes_{ΔRAC/Ssb-assembled}, complementation with purified RAC can restore the interaction of RAC with ES12 as well as the interaction of Ssb with nascent chains and by that reduce ribosome stalling on poly-AAG/A.

SUPPLEMENTARY DATA

Supplementary Data are available at NAR Online.

ACKNOWLEDGEMENTS

We thank Dr. Redmond Smyth for helpful discussions and valuable comments on the manuscript.

FUNDING

Deutsche Forschungsgemeinschaft [SFB 746, DFG RO 1028/5-2]; Excellence Initiative of the German Federal and State Governments [BIOSS-2 A9]. Funding for open access charge: Deutsche Forschungsgemeinschaft [DFG RO 1028/5-2].

Conflict of interest statement. None declared.

REFERENCES

1. Woolford, J.L. Jr. and Baserga, S.J. (2013) Ribosome biogenesis in the yeast *Saccharomyces cerevisiae*. *Genetics*, **195**, 643–681.
2. Turowski, T.W. and Tollervey, D. (2015) Cotranscriptional events in eukaryotic ribosome synthesis. *Wiley Interdiscip. Rev. RNA*, **6**, 129–139.
3. Rospert, S., Rakwalska, M. and Dubaquié, Y. (2005) Polypeptide chain termination and stop codon readthrough on eukaryotic ribosomes. *Rev. Physiol. Biochem. Pharmacol.*, **155**, 1–30.
4. Scheper, G.C., van der Knaap, M.S. and Proud, C.G. (2007) Translation matters: protein synthesis defects in inherited disease. *Nat. Rev. Genet.*, **8**, 711–723.
5. Dever, T.E. and Green, R. (2012) The elongation, termination, and recycling phases of translation in eukaryotes. *Cold Spring Harb. Perspect. Biol.*, **4**, a013706.
6. Brown, A., Shao, S., Murray, J., Hegde, R.S. and Ramakrishnan, V. (2015) Structural basis for stop codon recognition in eukaryotes. *Nature*, **524**, 493–496.
7. Dabrowski, M., Bukowy-Bieryllo, Z. and Zietkiewicz, E. (2015) Translational readthrough potential of natural termination codons in eucaryotes—The impact of RNA sequence. *RNA Biol.*, **12**, 950–958.
8. Chiabudini, M., Tais, A., Zhang, Y., Hayashi, S., Wölfe, T., Fitzke, E. and Rospert, S. (2014) Release factor eRF3 mediates premature translation termination on polylysine-stalled ribosomes in *Saccharomyces cerevisiae*. *Mol. Cell Biol.*, **34**, 4062–4076.
9. Sin, C., Chiarugi, D. and Valleriani, A. (2016) Quantitative assessment of ribosome drop-off in *E. coli*. *Nucleic Acids Res.*, **44**, 2528–2537.
10. Bonnin, P., Kern, N., Young, N.T., Stansfield, I. and Romano, M.C. (2017) Novel mRNA-specific effects of ribosome drop-off on translation rate and polysome profile. *PLoS Comput. Biol.*, **13**, e1005555.
11. Svidritskiy, E., Demo, G. and Korostelev, A.A. (2018) Mechanism of premature translation termination on a sense codon. *J. Biol. Chem.*, **293**, 12472–12479.
12. Wang, X., Xuan, Y., Han, Y., Ding, X., Ye, K., Yang, F., Gao, P., Goff, S.P. and Gao, G. (2019) Regulation of HIV-1 Gag-Pol expression by shiftless, an inhibitor of programmed -1 ribosomal frameshifting. *Cell*, **176**, 625–635.
13. Peisker, K., Chiabudini, M. and Rospert, S. (2010) The ribosome-bound Hsp70 homolog Ssb of *Saccharomyces cerevisiae*. *Biochim. Biophys. Acta*, **1803**, 662–672.
14. Zhang, Y., Sinning, I. and Rospert, S. (2017) Two chaperones locked in an embrace: structure and function of the ribosome-associated complex RAC. *Nat. Struct. Mol. Biol.*, **24**, 611–619.
15. Gautschi, M., Mun, A., Ross, S. and Rospert, S. (2002) A functional chaperone triad on the yeast ribosome. *Proc. Natl. Acad. Sci. U.S.A.*, **99**, 4209–4214.
16. Willmund, F., Del Alamo, M., Pechmann, S., Chen, T., Albanese, V., Dammer, E.B., Peng, J. and Frydman, J. (2013) The cotranslational function of ribosome-associated hsp70 in eukaryotic protein homeostasis. *Cell*, **152**, 196–209.

17. Döring, K., Ahmed, N., Riemer, T., Suresh, H.G., Vainshtein, Y., Habich, M., Riemer, J., Mayer, M.P., O'Brien, E.P., Kramer, G. *et al.* (2017) Profiling Ssb-Nascent chain interactions reveals principles of Hsp70-Assisted folding. *Cell*, **170**, 298–311.
18. Shiber, A., Döring, K., Friedrich, U., Klann, K., Merker, D., Zedan, M., Tippmann, F., Kramer, G. and Bukau, B. (2018) Cotranslational assembly of protein complexes in eukaryotes revealed by ribosome profiling. *Nature*, **561**, 268–272.
19. Albanese, V., Reissmann, S. and Frydman, J. (2010) A ribosome-anchored chaperone network that facilitates eukaryotic ribosome biogenesis. *J. Cell Biol.*, **189**, 69–81.
20. Shulga, N., James, P., Craig, E.A. and Goldfarb, D.S. (1999) A nuclear export signal prevents *Saccharomyces cerevisiae* Hsp70 Ssb1p from stimulating nuclear localization signal-directed nuclear transport. *J. Biol. Chem.*, **274**, 16501–16507.
21. Broach, J.R. (2012) Nutritional control of growth and development in yeast. *Genetics*, **192**, 73–105.
22. von Plehwe, U., Berndt, U., Conz, C., Chiabudini, M., Fitzke, E., Sickmann, A., Petersen, A., Pfeifer, D. and Rospert, S. (2009) The Hsp70 homolog Ssb is essential for glucose sensing via the SNF1 kinase network. *Genes Dev.*, **23**, 2102–2115.
23. Koplin, A., Preissler, S., Ilna, Y., Koch, M., Scior, A., Erhardt, M. and Deuerling, E. (2010) A dual function for chaperones SSB-RAC and the NAC nascent polypeptide-associated complex on ribosomes. *J. Cell Biol.*, **189**, 57–68.
24. Mudholkar, K., Fitzke, E., Prinz, C., Mayer, M.P. and Rospert, S. (2017) The Hsp70 homolog Ssb affects ribosome biogenesis via the TORC1-Sch9 signaling pathway. *Nat. Commun.*, **8**, 1–14.
25. Ogle, J.M., Carter, A.P. and Ramakrishnan, V. (2003) Insights into the decoding mechanism from recent ribosome structures. *Trends Biochem. Sci.*, **28**, 259–266.
26. Zaher, H.S. and Green, R. (2009) Fidelity at the molecular level: lessons from protein synthesis. *Cell*, **136**, 746–762.
27. Prokhorova, I., Altman, R.B., Djumagulov, M., Shrestha, J.P., Urzhumtsev, A., Ferguson, A., Chang, C.T., Yusupov, M., Blanchard, S.C. and Yusupova, G. (2017) Aminoglycoside interactions and impacts on the eukaryotic ribosome. *Proc. Natl. Acad. Sci. U.S.A.*, **114**, E10899–E10908.
28. Rakwalska, M. and Rospert, S. (2004) The Ribosome-Bound chaperones RAC and Ssb1/2p are required for accurate translation in *Saccharomyces cerevisiae*. *Mol. Cell Biol.*, **24**, 9186–9197.
29. Lee, K., Sharma, R., Shrestha, O.K., Bingman, C.A. and Craig, E.A. (2016) Dual interaction of the Hsp70 J-protein cochaperone Zuo1 with the 40S and 60S ribosomal subunits. *Nat. Struct. Mol. Biol.*, **23**, 1003–1010.
30. Brandman, O. and Hegde, R.S. (2016) Ribosome-associated protein quality control. *Nat. Struct. Mol. Biol.*, **23**, 7–15.
31. Koutmou, K.S., Schuller, A.P., Brunelle, J.L., Radhakrishnan, A., Djuranovic, S. and Green, R. (2015) Ribosomes slide on lysine-encoding homopolymeric A stretches. *Elife*, **4**, e05534.
32. Heitman, J., Movva, N.R., Hiestand, P.C. and Hall, M.N. (1991) FK 506-binding protein proline rotamase is a target for the immunosuppressive agent FK 506 in *Saccharomyces cerevisiae*. *Proc. Natl. Acad. Sci. U.S.A.*, **88**, 1948–1952.
33. Gautschi, M., Lilie, H., Fünfschilling, U., Mun, A., Ross, S., Lithgow, T., Rücknagel, P. and Rospert, S. (2001) RAC, a stable ribosome-associated complex in yeast formed by the DnaK-DnaJ homologs Ssz1p and zuo1. *Proc. Natl. Acad. Sci. U.S.A.*, **98**, 3762–3767.
34. Chiabudini, M., Conz, C., Reckmann, F. and Rospert, S. (2012) RAC/Ssb is required for translational repression induced by polylysine segments within nascent chains. *Mol. Cell Biol.*, **32**, 4769–4779.
35. Gueldener, U., Heinisch, J., Koehler, G.J., Voss, D. and Hegemann, J.H. (2002) A second set of loxP marker cassettes for Cre-mediated multiple gene knockouts in budding yeast. *Nucleic Acids Res.*, **30**, e23.
36. Kushnirov, V.V. (2000) Rapid and reliable protein extraction from yeast. *Yeast*, **16**, 857–860.
37. Garcia, P.D., Hansen, W. and Walter, P. (1991) In vitro protein translocation across microsomal membranes of *Saccharomyces cerevisiae*. *Methods Enzymol.*, **194**, 675–682.
38. Maniatis, T., Jeffrey, A. and van deSande, H. (1975) Chain length determination of small double- and single-stranded DNA molecules by polyacrylamide gel electrophoresis. *Biochemistry*, **14**, 3787–3794.
39. Raue, U., Oellerer, S. and Rospert, S. (2007) Association of protein biogenesis factors at the yeast ribosomal tunnel exit is affected by the translational status and nascent polypeptide sequence. *J. Biol. Chem.*, **282**, 7809–7816.
40. Schägger, H. and von Jagow, G. (1987) Tricine-sodium dodecyl sulfate-polyacrylamide gel electrophoresis for the separation of proteins in the range from 1 to 100 kDa. *Anal. Biochem.*, **166**, 368–379.
41. Sachs, M.S., Wang, Z., Gaba, A., Fang, P., Belk, J., Ganesan, R., Amrani, N. and Jacobson, A. (2002) Toeprint analysis of the positioning of translation apparatus components at initiation and termination codons of fungal mRNAs. *Methods*, **26**, 105–114.
42. Peattie, D.A. and Gilbert, W. (1980) Chemical probes for higher-order structure in RNA. *Proc. Natl. Acad. Sci. U.S.A.*, **77**, 4679–4682.
43. Caprara, M. (2013) RNA structure determination using chemical methods. *Cold Spring Harb. Protoc.*, **2013**, doi:10.1101/pdb.prot078485.
44. Keller, S., Vargas, C., Zhao, H., Piszczek, G., Brautigam, C.A. and Schuck, P. (2012) High-precision isothermal titration calorimetry with automated peak-shape analysis. *Anal. Chem.*, **84**, 5066–5073.
45. Brautigam, C.A., Zhao, H., Vargas, C., Keller, S. and Schuck, P. (2016) Integration and global analysis of isothermal titration calorimetry data for studying macromolecular interactions. *Nat. Protoc.*, **11**, 882–894.
46. Houtman, J.C., Brown, P.H., Bowden, B., Yamaguchi, H., Appella, E., Samelson, L.E. and Schuck, P. (2007) Studying multisite binary and ternary protein interactions by global analysis of isothermal titration calorimetry data in SEDPHAT: application to adaptor protein complexes in cell signaling. *Protein Sci.*, **16**, 30–42.
47. Brautigam, C.A. (2015) Calculations and Publication-Quality Illustrations for Analytical Ultracentrifugation Data. *Methods Enzymol.*, **562**, 109–133.
48. Passos, D.O., Doma, M.K., Shoemaker, C.J., Muhlrad, D., Green, R., Weissman, J., Hollien, J. and Parker, R. (2009) Analysis of Dom34 and its function in no-go decay. *Mol. Biol. Cell*, **20**, 3025–3032.
49. Inada, T. (2017) The ribosome as a platform for mRNA and nascent polypeptide quality control. *Trends Biochem. Sci.*, **42**, 5–15.
50. Dinman, J.D. (2012) Mechanisms and implications of programmed translational frameshifting. *Wiley Interdiscip. Rev. RNA*, **3**, 661–673.
51. Arthur, L., Pavlovic-Djuranovic, S., Smith-Koutmou, K., Green, R., Szczesny, P. and Djuranovic, S. (2015) Translational control by lysine-encoding A-rich sequences. *Sci. Adv.*, **1**, e1500154.
52. Arthur, L.L. and Djuranovic, S. (2018) PolyA tracks, polybasic peptides, poly-translational hurdles. *Wiley Interdiscip. Rev. RNA*, **9**, e1486.
53. Zhang, Y., Ma, C., Yuan, Y., Zhu, J., Li, N., Chen, C., Wu, S., Yu, L., Lei, J. and Gao, N. (2014) Structural basis for interaction of a cotranslational chaperone with the eukaryotic ribosome. *Nat. Struct. Mol. Biol.*, **21**, 1042–1046.
54. Anthony, D.D. and Merrick, W.C. (1992) Analysis of 40 S and 80 S complexes with mRNA as measured by sucrose density gradients and primer extension inhibition. *J. Biol. Chem.*, **267**, 1554–1562.
55. Wang, Z. and Sachs, M.S. (1997) Ribosome stalling is responsible for arginine-specific translational attenuation in *Neurospora crassa*. *Mol. Cell Biol.*, **17**, 4904–4913.
56. Pestova, T.V., Hellen, C.U. and Shatsky, I.N. (1996) Canonical eukaryotic initiation factors determine initiation of translation by internal ribosomal entry. *Mol. Cell Biol.*, **16**, 6859–6869.
57. Namy, O., Galopier, A., Martini, C., Matsufuji, S., Fabret, C. and Rousset, J.P. (2008) Epigenetic control of polyamines by the prion [PSI⁺]. *Nat. Cell Biol.*, **10**, 1069–1075.
58. Baudin-Baillieu, A., Fabret, C., Liang, X.H., Piekna-Przybylska, D., Fournier, M.J. and Rousset, J.P. (2009) Nucleotide modifications in three functionally important regions of the *Saccharomyces cerevisiae* ribosome affect translation accuracy. *Nucleic Acids Res.*, **37**, 7665–7677.
59. Hobbie, S.N., Kalapala, S.K., Akshay, S., Bruell, C., Schmidt, S., Dabow, S., Vasella, A., Sander, P. and Bottger, E.C. (2007) Engineering the rRNA decoding site of eukaryotic cytosolic ribosomes in bacteria. *Nucleic Acids Res.*, **35**, 6086–6093.

60. Fan-Minogue, H. and Bedwell, D.M. (2008) Eukaryotic ribosomal RNA determinants of aminoglycoside resistance and their role in translational fidelity. *RNA*, **14**, 148–157.
61. Gumiero, A., Conz, C., Gesé, G.V., Zhang, Y., Weyer, F.A., Lapouge, K., Kappes, J., von Plehwe, U., Schermann, G., Fitzke, E. *et al.* (2016) Interaction of the cotranslational Hsp70 Ssb with ribosomal proteins and rRNA depends on its lid domain. *Nat. Commun.*, **7**, 13563.
62. Sloan, K.E., Warda, A.S., Sharma, S., Entian, K.D., Lafontaine, D.L.J. and Bohnsack, M.T. (2017) Tuning the ribosome: the influence of rRNA modification on eukaryotic ribosome biogenesis and function. *RNA Biol.*, **14**, 1138–1152.
63. Decatur, W.A. and Fournier, M.J. (2002) rRNA modifications and ribosome function. *Trends Biochem. Sci.*, **27**, 344–351.
64. Liang, X.H., Liu, Q. and Fournier, M.J. (2007) rRNA modifications in an intersubunit bridge of the ribosome strongly affect both ribosome biogenesis and activity. *Mol. Cell*, **28**, 965–977.
65. Baxter-Roshek, J.L., Petrov, A.N. and Dinman, J.D. (2007) Optimization of ribosome structure and function by rRNA base modification. *PLoS One*, **2**, e174.
66. Jack, K., Bellodi, C., Landry, D.M., Niederer, R.O., Meskauskas, A., Musalgaonkar, S., Kopmar, N., Krasnykh, O., Dean, A.M., Thompson, S.R. *et al.* (2011) rRNA pseudouridylation defects affect ribosomal ligand binding and translational fidelity from yeast to human cells. *Mol. Cell*, **44**, 660–666.
67. Piekna-Przybylska, D., Decatur, W.A. and Fournier, M.J. (2007) New bioinformatic tools for analysis of nucleotide modifications in eukaryotic rRNA. *RNA*, **13**, 305–312.
68. Esguerra, J., Warringer, J. and Blomberg, A. (2008) Functional importance of individual rRNA 2'-O-ribose methylations revealed by high-resolution phenotyping. *RNA*, **14**, 649–656.
69. Shalev-Benami, M., Zhang, Y., Rozenberg, H., Nobe, Y., Taoka, M., Matzov, D., Zimmerman, E., Bashan, A., Isobe, T., Jaffe, C.L. *et al.* (2017) Atomic resolution snapshot of *Leishmania* ribosome inhibition by the aminoglycoside paromomycin. *Nat. Commun.*, **8**, 1589.
70. Hatin, I., Fabret, C., Namy, O., Decatur, W. and Rousset, J.P. (2007) Fine tuning of translation termination efficiency in *Saccharomyces cerevisiae* involves two factors in close proximity to the exit tunnel of the ribosome. *Genetics*, **177**, 1527–1537.
71. Liang, X.H., Liu, Q. and Fournier, M.J. (2009) Loss of rRNA modifications in the decoding center of the ribosome impairs translation and strongly delays pre-rRNA processing. *RNA*, **15**, 1716–1728.
72. Peisker, K., Braun, D., Wölflé, T., Hentschel, J., Fünfschilling, U., Fischer, G., Sickmann, A. and Rospert, S. (2008) Ribosome-associated complex binds to ribosomes in close proximity of Rpl31 at the exit of the polypeptide tunnel in yeast. *Mol. Biol. Cell*, **19**, 5279–5288.
73. Al-Hadid, Q., Roy, K., Chanfreau, G. and Clarke, S.G. (2016) Methylation of yeast ribosomal protein Rpl3 promotes translational elongation fidelity. *RNA*, **22**, 489–498.
74. Soulard, A., Cohen, A. and Hall, M.N. (2009) TOR signaling in invertebrates. *Curr. Opin. Cell Biol.*, **21**, 825–836.
75. Boguta, M. (2013) Maf1, a general negative regulator of RNA polymerase III in yeast. *Biochim. Biophys. Acta.*, **1829**, 376–384.
76. Courtes, F.C., Gu, C., Wong, N.S., Dedon, P.C., Yap, M.G. and Lee, D.Y. (2014) 28S rRNA is inducibly pseudouridylated by the mTOR pathway translational control in CHO cell cultures. *J. Biotechnol.*, **174**, 16–21.
77. Dontsova, O.A. and Dinman, J.D. (2005) 5S rRNA: structure and function from head to toe. *Int. J. Biomed. Sci.*, **1**, 1–7.
78. Tsuboi, T., Kuroha, K., Kudo, K., Makino, S., Inoue, E., Kashima, I. and Inada, T. (2012) Dom34:hbs1 plays a general role in quality-control systems by dissociation of a stalled ribosome at the 3' end of aberrant mRNA. *Mol. Cell*, **46**, 518–529.
79. Winz, M.L., Peil, L., Turowski, T.W., Rappsilber, J. and Tollervey, D. (2019) Molecular interactions between Hel2 and RNA supporting ribosome-associated quality control. *Nat. Commun.*, **10**, 563.
80. Sitron, C.S., Park, J.H. and Brandman, O. (2017) Asc1, Hel2, and Slh1 couple translation arrest to nascent chain degradation. *RNA*, **23**, 798–810.
81. Joazeiro, C.A.P. (2017) Ribosomal stalling during translation: providing substrates for ribosome-associated protein quality control. *Annu. Rev. Cell Dev. Biol.*, **33**, 343–368.
82. Ito-Harashima, S., Kuroha, K., Tatematsu, T. and Inada, T. (2007) Translation of the poly(A) tail plays crucial roles in nonstop mRNA surveillance via translation repression and protein destabilization by proteasome in yeast. *Genes Dev.*, **21**, 519–524.
83. Lu, J. and Deutsch, C. (2008) Electrostatics in the ribosomal tunnel modulate chain elongation rates. *J. Mol. Biol.*, **384**, 73–86.
84. Letzring, D.P., Wolf, A.S., Brule, C.E. and Grayhack, E.J. (2013) Translation of CGA codon repeats in yeast involves quality control components and ribosomal protein L1. *RNA*, **19**, 1208–1217.
85. Juszkievicz, S. and Hegde, R.S. (2017) Initiation of quality control during Poly(A) translation requires site-specific ribosome ubiquitination. *Mol. Cell*, **65**, 743–750.